Damage assessment by automated quantitative image analysis – a risky undertaking

P. Stroeven
Faculty of Civil Engineering and Geosciences,
Delft University of Technology, The Netherlands

Abstract

This paper presents the economic concept of describing damage in concrete by a partially linear planar system. The practical cases are elaborated of prevailing compressive or tensile stresses. They only require quantitatively analyzing the image patterns of vertical sections by sweeping test lines. Further it is demonstrated that automation of quantitative image analysis generally yields biased information.

Keywords: concrete, image analysis, automation, sweeping test line, vertical section.

1 Introduction

Concretes are undergoing a process of degradation during the lifetime of the engineering structure. The degree of degradation can be reflected by characteristics of the internal damage structure. Nature of this problem is three dimensional (3D). To get access to the relevant 3D information would require a random set of section images, which is a laborious and time consuming operation. So, most investigations are of 2D nature only. A method introduced by the author renders possible reducing such efforts tremendously [1–3]. It assumes the crack structure for the most general case composed of 3D, 2D and 1D portion. The method is therefore discussed for the practical case of concrete under prevailing compressive stresses and prevailing tensile stresses, respectively. Damage characteristics under such conditions can be assessed on a single so-called *vertical* section. A parallel set of such sections can be necessary of course to reduce scatter to acceptable proportions. However, the efforts for sawing and quantitative image analysis are obviously dramatically reduced.

WIT Transactions on Modelling and Simulation, Vol 48, © 2009 WIT Press
www.witpress.com, ISSN 1743-355X (on-line)
doi:10.2495/CMEM090171

The images of such vertical sections can be analyzed by the direct secants approach [4–9], whereby the number of intersections is determined per unit of line length for a stepwise rotating grid of parallel lines. Information can be obtained on total crack length per unit of area and on degree and direction of crack orientation. This is 2D information; however it is readily possible without investment of extra labour to assess the 3D specific crack surface area, and spatial orientation distribution of the cracks. This will be elaborated for the aforementioned practical cases. Due to the repetitive character of such investigations, one would be tempted to use an automated set up. However, the paper will demonstrate information generally to be seriously biased [10, 11]. This will be accomplished mathematically as well as by a visualization method proposed by Underwood [12]. This approach gives detailed insight into the level of bias as a function of conditions, such as the degree of prevailing orientation in the damage structure.

Since damage is a fractal phenomenon, the obtained results will fundamentally be a function of magnification of the images. This allows performing a comparative study only.

2 Damage assessment

The damage structure according to the Stroeven concept [13] is denoted as a partially linear-planar structure. The 3D portion encompasses small flat crack element dispersed isotropic uniformly random (IUR) in space. In the 2D portion only small crack elements are collected that are parallel to an orientation plane, however otherwise they are "randomly" distributed. The 1D portion unites crack elements all parallel to an orientation axis, however otherwise "randomly" dispersed. When the 2D portion can be neglected, a so-called *partially linearly oriented* system is obtained. This model can be used in situations where compressive stresses are prevailing. Alternatively, for high tensile stresses the *partially planar oriented* damage model can be employed in which the 1D portion is neglected. Damage can be seen as surfaces distributed in space (representing the two crack surfaces at very small distances). Crack density is commonly expressed in total surface area, S, per unit of volume, V. So, leading descriptor of the damage structure is S_V (in mm^{-1}). Alternatively, in 2D the total crack length, L, per unit of area, A, yields information on L_A. Measurements are made by superposition of line grids on images, of which fig. 1 (left) reveals only a small part (pore is visible at the bottom). Contrast was improved by applying a fluorescent spray. This author has extensively used this method of directed secants in the past 30 years. Incidentally, also other researchers in concrete technology used the very method [14–17]. Fig. 1 (right) shows grid orientations on a full-size hand-made copy of section image. Larger aggregate grains are visible as crack-free areas.

2.1 Concrete in compression

Uniaxial compressive stresses produce predominantly cracks that are parallel to the stress direction. In a more general set up, we assume a portion of cracks

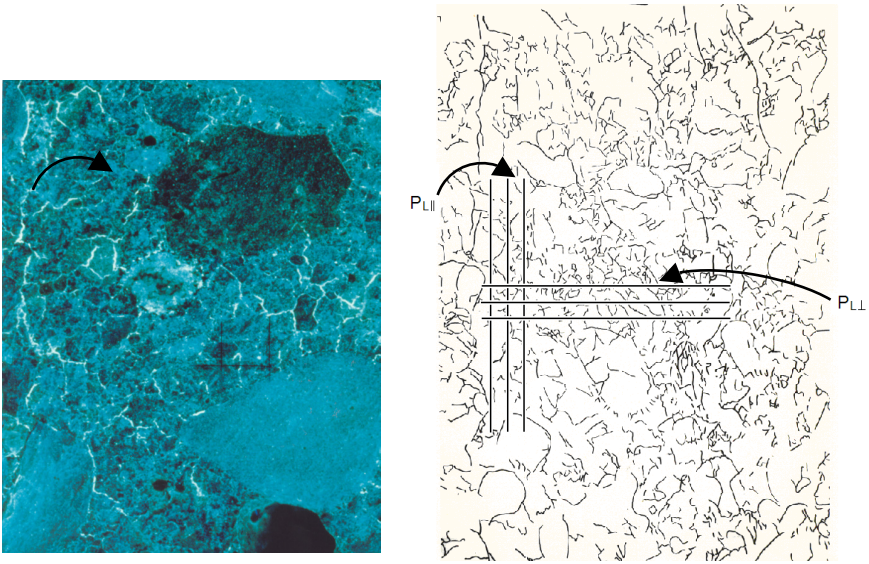

Figure 1: Load-induced cracks in section plane visualized by fluorescent spray (left), and application of method of directed secants for assessment of intersection densities (right).

distributed isotropic uniformly random (IUR); this is denoted as the S_{V3} component. The resulting portion consists of cracks parallel to the orientation axis, denoted as the S_{V1} component. Total crack density is the summation of both components: $S_{V1} + S_{V3} = S_V$. The proper approach (in technical as well as economic terms) is sampling by *vertical sections*. Hence, the specimen should be cut to yield one or more image planes parallel to the orientation axis. Such section images can provide the 3D information on S_V. Averaging over more vertical images reduces the scatter around the average, and thus the reliability of the results. The results are unbiased, which means that averaging over an increasing number of images will bring the average closer and closer to the population value we are interested in. The analysis of the images is accomplished by line scanning. A grid of parallel lines is superimposed on the crack pattern, successively in the direction of the orientation axis (indicated by index $\|$) and perpendicular to it (indicated by index $\perp$), as shown in fig. 1. The following relationships can be derived

$$P_{L\|} = \frac{1}{2} S_{V3} \quad \text{and} \quad P_{L\perp} = \frac{1}{2} S_{V3} + \frac{2}{\pi} S_{V1} \tag{1}$$

Hence, crack density is obtained by simple mathematical manipulations, yielding

$$S_V = \frac{\pi}{2} P_{L\perp} + (2 - \frac{\pi}{2}) P_{L\parallel} \tag{2}$$

P in eqs. (1) and (2) stands for the number of intersections of grid lines and cracks. The constants account for probabilities that cracks appear in the section image [6,7].

2.2 Concrete in tension

The methodology is very similar. The vertical section is again parallel to the tensile stresses. The grid is also successively superimposed in the stress direction and perpendicular to it, with the same indices accounting for the position of the grid. In this case we have

$$P_{L\parallel} = \frac{1}{2} S_{V3} + S_{V2} \quad \text{and} \quad P_{L\perp} = \frac{1}{2} S_{V3} \tag{3}$$

Again, simple manipulation will yield

$$S_V = S_{V2} + S_{V3} = P_{L\parallel} + P_{L\perp} \tag{4}$$

Here, S_{V2} stands for the portion of cracks perpendicular to the tensile stresses, with $S_V = S_{V2} + S_{V3}$. To accomplish such operations, the contrast should be improved by ink penetration or by application of a fluorescent spray (applied in the case of fig. 1) or dye. Details can be found in the relevant literature [5,8].

3 Biases due to automated set up

3.1 Analogue images

An elegant way to reveal differences in outcomes of quantitative image analysis approaches by directs secants to analogue and digitised images is to make use of the earlier mentioned Stroeven concept. Hence, L_A is assumed consisting of two portions, a "random" one, denoted by L_{Ar}, and a fully oriented one, indicated by L_{Ao}. The latter "sticks" (short straight elements as part of the 2D crack) run parallel to the orientation axis that supposedly makes an angle β with the positive *x*-axis. This strategy allows dealing with both portions separately. The rose of intersections per unit of grid line length (intersection densities) of the random portion approximates (for very large images) a circle around the origin with radius P_{Lr}. The rose of intersection densities for the oriented portion approximates a circle through the origin with $P_{Lo}(\beta) = 0$ and $P_{Lo}(\varsigma) = P_{Lo\max}$. Note that $\beta = \varsigma + \pi/2$. $P_{Lo}(\theta) = P_{Lo\max} \left|\cos(\theta - \varsigma)\right|$ for an arbitrary angle θ. When combined, the rose of intersection densities is obtained for a partially linear structure of lineal features in a plane, shown in fig. 3 [10].

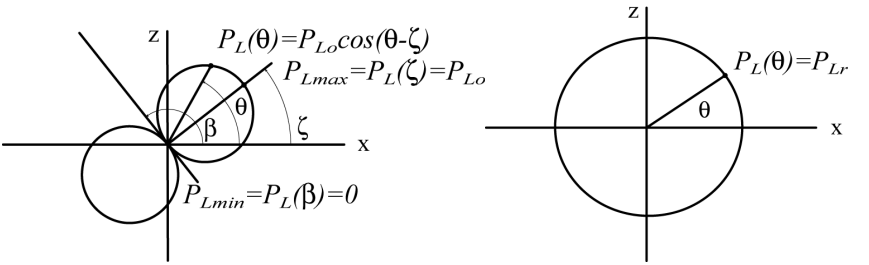

Figure 2: Rose of intersection densities for oriented (left) and random (right) line segments in a plane (together forming the 2D crack pattern) for an analogue image.

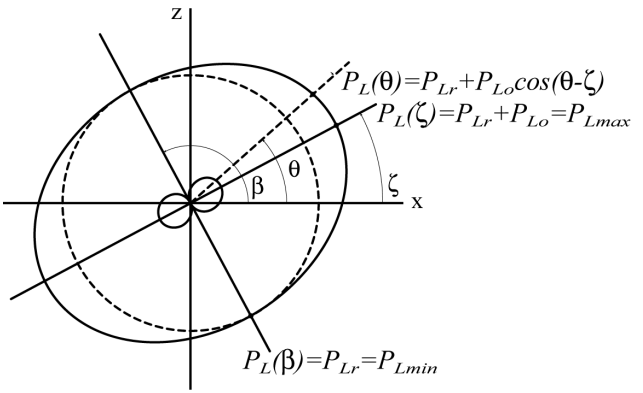

Figure 3: Rose of intersection densities for random (dashed line) plus oriented line segments in a plane (continuous line; small circles) shown in fig. 2. Crack pattern is supposed to encompass only relatively small lineal portion (so-called weakly oriented pattern).

3.2 Digitized images

The smooth contours of the cracks can be conceived in conventionally digitized images replaced by two orthogonal sets of mono-size sticks as shown in fig. 4. As before, a distinction can be made between the "random" portion and the oriented one running parallel to an orientation axis enclosing an angle β with the positive x-axis. As before, $\beta = \varsigma + \pi/2$. The random portion consists of two equally large sub-sets of sticks oriented in the respective coordinate directions $\{x,z\}$. This leads to two equally large roses of intersection densities that run through the origin and are orthogonally oriented. Circle diameter is P_{Lr}. The summation yields a symmetric flower-like rose displayed in fig. 5 at the bottom. In an arbitrary direction, the intersection density is given by

$$P_{Lr}(\theta) = P_{Lr}(\sin\theta + \cos\theta) = \sqrt{2}P_{Lr}\left|\cos(\theta - \frac{\pi}{4})\right| \tag{5}$$

A striking but expected observation is the preferred orientation in a direction enclosing an angle π/4 with the positive x-axis; the random portion is reflected significantly biased by a digitised image with maximum value $\sqrt{2}P_{Lr}$.

The projected portions of the oriented fraction of the cracks in the *x*- and *z*-directions are $L_A^{'}(0) = L_{Ao}\sin\varsigma$ and $L_A^{'}(\pi/2) = L_{Ao}\cos\varsigma$, respectively. This can be transformed to intersection counts per unit of grid line length, whereby the horizontal system of oriented sticks leads to two circles sharing the origin of the polar system and having the *z*-axis as symmetry line. The intersection with the *z*-axis is $P_{Lo}\sin\varsigma$. The second system of oriented sticks parallel to the z-axis is modelled in an analogous way by two circles sharing the origin of the polar system and having the *x*-axis as symmetry line. The intersection with *x*-axis is $P_{Lo}\cos\varsigma$. The two pairs of circles and their summation is displayed in fig. 5 (top). The intersection density in an arbitrary direction of the oriented portion is

$$P_{Lo}(\theta) = P_{Lo}\sin\theta\sin\varsigma + P_{Lo}\cos\theta\cos\varsigma = P_{Lo}\left|\cos(\theta - \varsigma)\right| \tag{6}$$

The direction of the principal axis of the rose is found for zero value of the first derivative of eqn. (6). This occurs for $\theta = \varsigma$, whereby $P_{Lo}(\varsigma) = P_{Lo}$.

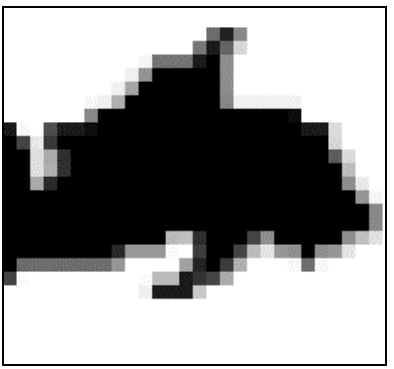

Figure 4: Detail of conventionally digitized section image of particulate structure of which the surfaces like cracks are dispersed in 3D space. Smooth surface contours are replaced by orthogonal set of straight line segments.

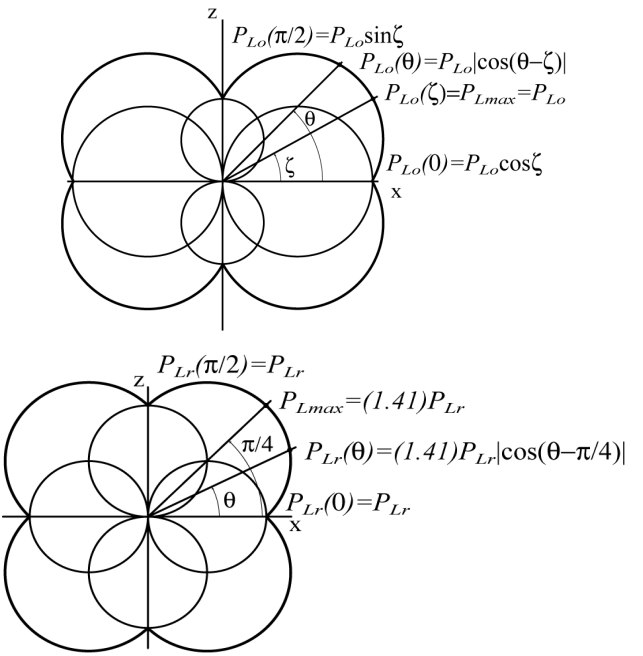

Figure 5: Rose of $P_L(\theta)$ values for oriented (top) and random (bottom) line segments in digitized image of crack pattern.

The roses for the partially oriented lineal crack features are obtain by summation of the total roses at the top and bottom of fig. 5. The mathematical expression for this system is obtained upon adding up Eqs. (5) and (6). In both cases it becomes obvious that the direction of preferred orientation, $\beta = \varsigma + \pi/2$, is only reflected by the experimental data *when the signal is very strong* (*i.e.*, $P_{Lo} / P_{lr} \gg 1$); when weak, the preferred orientation direction will be very close to $\pi/4$. Intermediate situations will be *biased to an unknown degree* when used for predicting the direction of preferred orientation.

4 Discussion

A more detailed insight into differences between quantitative image analysis outcomes obtained on either analogue or digitized images can be achieved by superimposing the relevant estimates assessed on the different images for the fully oriented and random portions *separately*. Fig. 6 (top) presents the fully oriented portions as reflected by the two approaches. In the first and third quadrant the solutions are identical, whereas they are distinctly different in the other two quadrants. Digitized images only offer correct information along the axes of (four-connexity) digitization (fig. 6: bottom). All other measurements

will be biased to an unknown degree. Only when confronted with very strong signals one might successfully assess such geometric parameters by an automated approach to digitized images. By equating the first derivative to zero of the aforementioned expression for the analogue and digitized images, this is confirmed by the respective equations that are obtained (in the first quadrant): $P_{Lo}\sin(\theta-\varsigma)=0$ and $P_{Lo}\sin(\theta-\varsigma)+\sqrt{2}P_{Lr}\sin(\theta-\pi/4)=0$, for analogue and digitized images, respectively. The correct solution ($\theta=\varsigma$) is only for the analogue image.

Estimation of total length of lineal features in a plane, L_A, is based on $L_A=\frac{\pi}{2}\overline{P}_L(\theta)=\frac{\pi}{2}\int_0^{\pi}[P_{Lo}\cos(\theta-\varsigma)+\sqrt{2}P_{Lr}\cos(\theta-\frac{\pi}{4})]d\theta/\int_0^{\pi}d\theta$. This holds for analogue as well as for digitized images. The respective solutions are

$$L_A=\frac{\pi}{2}P_{Lr}+P_{Lo}\ \text{(anal.)}\quad\text{and}\quad L_A=\sqrt{2}\cos(\varsigma-\frac{\pi}{4})P_{Lo}+2P_{Lr}\ \text{(digit.)}\quad(7)$$

L_A as obtained from digitized image is *always biased* (*i.e.*, overestimated); even for very strong signals, the ratio of digitized to analogue image information

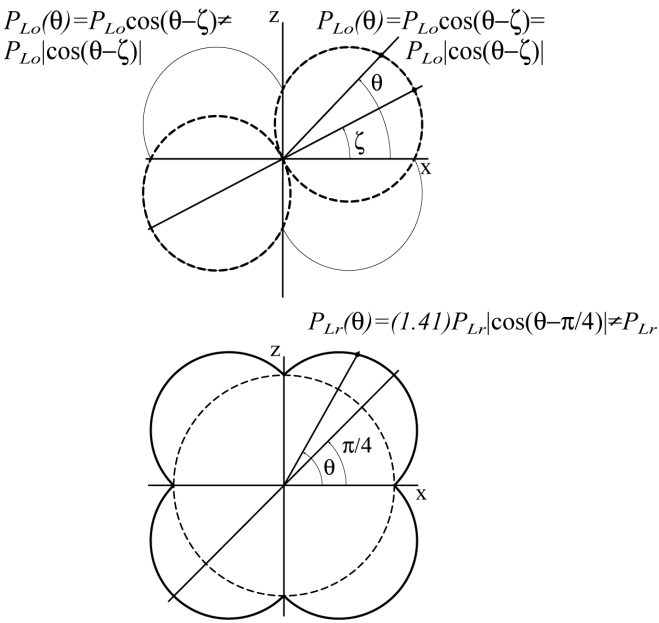

Figure 6: Digitization-induced biases for oriented (top) and random portion (bottom) of rose of intersection densities. Dashed line represents the analogue image, the solid line the digitized image subjected to the automated model.

is $\sqrt{2}\cos(\varsigma - \pi/4)$. For very weak signals this yields $4/\pi$. For mixed situations, the bias can be anywhere between $\sqrt{2}$ and $4/\pi$, with even an influence of the direction of preferred orientation.

A parameter used to characterize the *strength* of preferred orientation is the *degree of orientation, ω*. This parameter can be derived for a space system (ω_3), as well as for a planar one (ω_2) by the information in this paper. As an example, for ω_2 this leads to

$$\omega_2 = \frac{P_{Lo}.100}{1.572P_{Lr} + P_{Lo}} = \frac{100}{1.572\dfrac{P_{Lr}}{P_{Lo}} + 1} \ (\%) \quad \text{(analogue)} \tag{8}$$

$$\omega_2 = \frac{1 + \dfrac{P_{Lr}}{P_{Lo}}[1 - 1.73\cos(\varsigma + \dfrac{\pi}{4})]}{1 + \dfrac{P_{Lr}}{P_{Lo}}[1 + \cos(\varsigma + \dfrac{\pi}{4})]} 100 \ (\%) \quad \text{(digitized)} \tag{9}$$

The correct signal for the analogue image declines smoothly from strong to weak signals from 100% to 0%. For the digitized image it declines also from 100% for strong signals to anywhere between 100% and 0%, depending on the orientation direction in the image field, for weak signals. So, information will generally be biased to an unknown degree.

5 Conclusions

Spatial damage structures can be analyzed by application of quantitative image analysis by sweeping test line system on orthogonal section images only. For the practical cases of prevailing compressive or tensile loadings, (a set of) vertical sections will do, restricting dramatically efforts required for preparation of samples and image analysis.

The choice to automate the quantitative image analysis operation is a risky one, because characteristic measures for the damage structure, like total crack length (or specific crack surface area) and degree and direction of prevailing crack orientation will be seriously biased.

References

[1] Stroeven, P., Shah, S.P., Use of radiography-image analysis for steel fiber reinforced concrete, *Testing and Test Methods of Fiber Cement Composites*, ed. R.N. Swamy, Constr. Press: Lancaster, pp. 345-353, 1978.

[2] Stroeven, P., de Haan, Y.M., Structural investigations on steel fiber reinforced concrete, *High Performance Reinforced Cement Composites*, eds. H.W. Reinhardt, A.E. Naaman, E & FN Spon: London, pp. 407-418, 1992.

[3] Stroeven P., Damage evolution in concrete; application of stereology to quantitative image analysis and modelling, *Advanced Materials for Future Industries: Needs and Seeds*, eds. Kimpara I, Kageyama K, Kagawa Y, SAMPE: Tokyo, pp. 1436-1443, 1991.
[4] Nemati, K.M., Stroeven, P., Stereological analysis of micro-mechanical behaviour of concrete. *Mat. Struct*. **34**, pp. 486-494, 2000.
[5] Reinhardt, H.W., Stroeven, P., den Uijl, J.A., Kooistra, T.R., Vrencken, J.H.A.M., Einfluss von Schwingbreite, Belastungshöhe und Frequenz auf die Schwingfestigkeit von Beton bei niedrigen Bruchlastwechselzahlen. *Betonw. & Fertigteil-Techn*., **44,** pp. 498-503, 1978.
[6] Stroeven, P., Hu, J., Gradient structures in cementitious materials, *Cem. Concr. Comp.*, **29**, pp. 313-323, 2007
[7] Stroeven, P., Hu, J., Stereology: Historical perspective and applicability to concrete technology, *Mat. Struct*., **39,** pp.127-135, 2005.
[8] Stroeven, P., Some observations on microcracking in concrete subjected to various loading regimes, *Engr. Fract. Mech*., **35**(4/5), pp.775-782, 1990.
[9] Stroeven P., Geometric probability approach to the examination of microcracking in plain concrete, *J. Mat. Sc.* **14**, pp.1141-1151, 1979.
[10] Stroeven, P., Stroeven, A.P., Dalhuisen, D.H., Image Analysis of 'natural' concrete samples by automated and manual procedures, *Cem. Concr. Comp.***, 23**, pp. 227-236, 2001.
[11] Chaix, J.M., Grillon, F., On the rose of direction measurements on the discrete grid of an automatic image analyser, *J. Microsc*., **184,** pp. 208-213,1996.
[12] Underwood E.E., *Quantitative Stereology*, Addison-Wesley: Reading (MA), 1970.
[13] Stroeven, P., Structural modelling of plain and fibre reinforced concrete, *J. Comp.*, **13**, pp. 129-139, 1982.
[14] Stang, H., Mobasher, B., Shah, S.P., Quantitative damage characterization in polypropylene fibre reinforced concrete, *Cem. Concr. Res*., **20**, pp. 540-558, 1990.
[15] Carcassès, M., Ollivier, J.P., Ringot, E., Analysis of microcracking in concrete, *Acta Stereol*., **8**(2), pp. 307-312, 1989.
[16] Ringot, E., Automatic quantification of microcracks network by stereological method of total projections in mortars and concrete, *Cem. Concr. Res.*, **18**, pp. 35-43,1988.
[17] Nemati, K.M., *Generation and interaction of compressive stress-induced microcracks in concrete*, PhD Thesis, University of California: Berkeley, 1994.